A TECHNIQUE TO CALIBRATE NONLINEAR CAR-FOLLOWING LAWS FOR TRAFFIC OSCILLATION ESTIMATION

BY

CHRISTINE M. RHOADES

THESIS

Submitted in partial fulfillment of the requirements
for the degree of Master of Science in Civil Engineering
in the Graduate College of the
University of Illinois at Urbana-Champaign, 2015

Urbana, Illinois

Adviser:

Associate Professor Yanfeng Ouyang

ABSTRACT

Traffic congestion is one of the chief transportation problems in the world today. The total cost of transportation congestion in the United States in 2011 was estimated at 121 billion dollars. Congested traffic rarely flows smoothly; instead, traffic goes through cyclical slow and fast movements that result in what is commonly known as traffic oscillations. There are numerous negative effects associated with these oscillations, including extra fuel consumption and greenhouse gas emissions. Therefore, transportation professionals would like to find a way to reduce traffic oscillations.

Hence, researchers have developed numerous models to help reproduce traffic oscillations, in the hopes of better understanding how oscillations form and propagate through a platoon of vehicles. Many simulation and experimental studies have been performed to study oscillations, but as data collection technologies have improved, they have provided the opportunity to study oscillations as they occur in the real world. By calibrating the parameters of the theoretical models with empirical data, it is possible to more accurately reproduce driver behavior in oscillations and consequently to evaluate the impacts of various potential traffic control strategies on traffic oscillations.

This thesis proposes a calibration technique that is useful in calibrating nonlinear car-following laws to accurately model traffic oscillations from field trajectory data in both the time domain and the frequency domain. The base of the technique is maximum likelihood estimation, as calculated using the speed-spacing diagram. Time-domain and frequency-domain feedback is then added to this base to achieve accuracy in both domains. Numerical examples using NGSIM data (Next Generation SIMulation) are provided to verify the proposed method. Further analysis of the model parameters and potential traffic control strategies to mitigate the traffic oscillation problem are then discussed.

ACKNOWLEDGMENTS

This work would not have been possible without the support of many people. A special thanks to my adviser, Yanfeng Ouyang, who patiently directed me in my research and then guided me through this process. Many thanks to Xin Wang, the PhD student who collaborated with me, for always being willing to lend a helping hand. Thanks also to my research group, whose questions and comments helped improve my work, and especially to Xin Wang and Laura Ghosh for taking the time to read through my thesis and offer suggestions to improve it.

Thanks to my friends at 312 House and UBC, who have been a tremendous source of encouragement for the past few years. Many thanks also to my parents and family, Jerry and Mary, Jason, Jennifer, and Amanda. They have always been there to listen and offer support or advice. Finally, I would like to thank God for giving me this opportunity and then leading me through it, providing encouragement and peace when I needed it most.

TABLE OF CONTENTS

CHAPTER 1
INTRODUCTION

1.1. Background

Traffic congestion is the chief transportation problem in major cities around the world. Schrank et al. (2012) report that in 2011, 5.5 billion hours and 2.9 billion gallons of fuel were wasted and approximately 56 billion extra pounds of carbon dioxide were produced in the United States in congested traffic. In 2011, the total cost of congestion in the United States was estimated at 121 billion dollars (Scrank et al., 2012). These numbers are only for 498 urban areas in the United States, so it is easy to see that, on a worldwide scale, traffic congestion is a massive problem with huge economic and environmental repercussions, as well as implications for efforts to conserve natural resources.

For years, traffic engineers and researchers have tried various strategies to address the problem of traffic congestion. Although some solutions, such as adding capacity, can temporarily help mitigate congestion, no solutions have been found to completely eliminate traffic congestion in the long run. It seems that traffic congestion is here to stay. Indeed, as populations continue to grow and car ownership rates continue to increase, it is expected that traffic congestion will continue to worsen in the future.

Thus, many transportation researchers have studied traffic congestion, trying to determine its causes and potential strategies to combat it. One well-known characteristic of congested traffic is the turbulence of its flow. Instead of flowing smoothly, congested traffic often fluctuates between fast and slow movements, leading to what is known as traffic oscillations. In the extreme case, the gridlocked situations often pictured when the words “congested traffic” are heard, this fluctuation leads to what is commonly called stop-and-go traffic, which forces drivers to periodically come to a complete stop. Schrank et al. (2012) estimates that the capacity of roads with turbulent flow can be effectively reduced by a factor as large as one-half. Therefore, it seems apparent that traffic oscillations can worsen or even cause congested traffic conditions, making it essential to understand this phenomenon.

Traffic oscillations can easily be studied and visualized using the time-space plane (Laval, 2011). For example, Figure 1 shows the time-space diagram for congested traffic that experiences traffic oscillations. It can be seen that the vehicle trajectories are not all straight lines, which would be a sign of stable traffic flow. Instead, many trajectories have a curved segment, indicating the temporary deceleration followed by acceleration that is often seen in unstable traffic flow. Some trajectories even have a flat segment, which means the vehicle had to come to a complete stop.

Figure 1 also illustrates the formation and propagation of oscillations through a platoon of vehicles. The oscillation starts as a small perturbation in one trajectory that is then amplified upstream through the platoon until it develops into a large oscillation that may eventually cause traffic to come to a complete standstill. Here, the time-space diagram shows that most trajectories only experience one oscillation period within the data collection zone, but it can also be seen that three different waves of oscillations form and propagate.

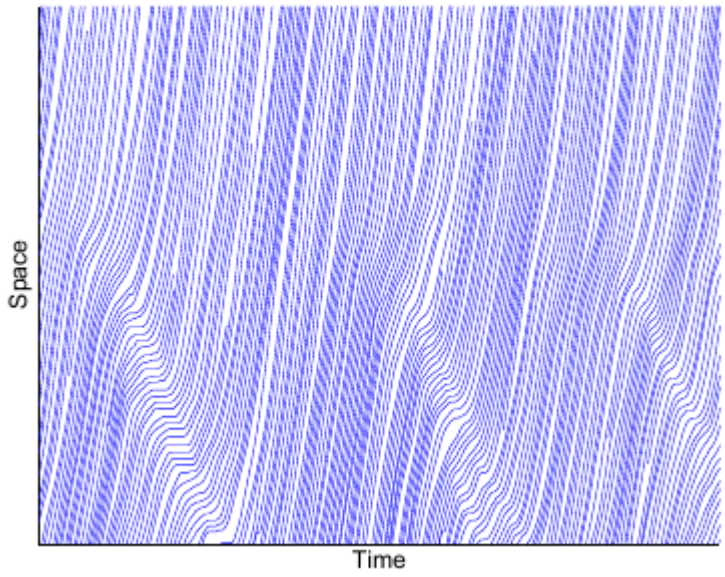

Figure 1: Time-space diagram showing traffic oscillations (source: NGSIM data; source: http:ngsim.fhwa.dot.gov/)

There are numerous negative effects associated with traffic oscillations. Traffic oscillations pose a safety hazard due to the repeated changes in traffic speed. Crashes are likely to occur when drivers are not vigilant or when they are simply unable to react quickly enough to the repeatedly changing speeds. Zheng et al. (2010) report that oscillations significantly increase

the number of crashes on a road; in their study, one unit increase in the standard deviation of freeway speed is associated with an 8% increase in the probability of a rear-end collision.

The necessity of heightened awareness and the periodic slow-downs also lead to driver frustration. Slower speeds cause additional travel delay, and the cyclical accelerations and decelerations result in extra fuel consumption and greenhouse gas emissions. Thus, traffic oscillations can negatively affect drivers physically, mentally, and financially. When examined on a broader scale, traffic oscillations cause problems for society as a whole by negatively impacting the environment.

Due to the widespread nature of traffic congestion and the variety of negative effects associated with the resulting traffic oscillations, there has been a strong motivation for researchers and practitioners alike to study this phenomenon. It is expected that by developing a better understanding of traffic oscillations, including both the way they start and the way they propagate, a strategy will be found that can help mitigate oscillations and their effects.

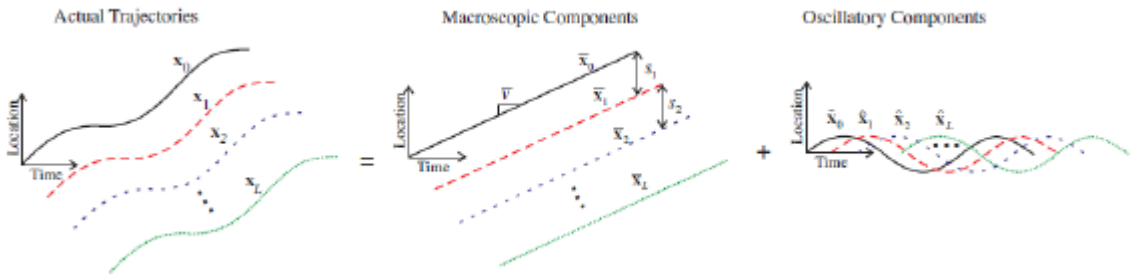

Figure 2: Trajectory decomposition (source: Li et al., 2012)

1.2. Current Work

Traffic oscillations can be studied in the time domain or the frequency domain. In particular, trajectory data with oscillations can be decomposed into their corresponding macroscopic components and oscillatory components, as seen in Figure 2 (Li et al., 2010). The macroscopic component, easily studied in the time domain, reflects macroscopic traffic properties such as average speed, spacing, and flow. The oscillatory component reflects the properties of the oscillations such as the period and amplitude of oscillation and can be more

effectively studied using frequency-domain methods. Hence, there have been numerous efforts to model traffic oscillations either in the time domain or the frequency domain, separately.

This paper fills an important gap by detailing a new technique to calibrate a nonlinear car-following law to accurately model traffic oscillations in both the time and frequency domains. With the advent of new data collection technologies, better quality field trajectory data showing oscillations in the real world have become available. This paper uses NGSIM field data (Next Generation SIMulation; source: http:ngsim.fhwa.dot.gov/) to calibrate a nonlinear car-following law that is able to not only reproduce the observed trajectories in the time-space diagram but also to predict the oscillation propagation through the platoon of vehicles using frequency-domain methods.

The ability to model traffic oscillations is critical in understanding them and working towards a mitigation strategy, since it provides researchers with the opportunity to explore how potential traffic control strategies may affect the oscillations and to evaluate their effectiveness. The paper is therefore organized as follows. Chapter 2 provides a literature review that covers relevant research, including the history and the current state of traffic oscillations research. Chapter 3 then describes the proposed car-following model calibration technique, based on a maximum likelihood estimation approach along with feedback from time- and frequency-domain calibration errors. Further analyses and potential ways to mitigate oscillations are discussed in Chapter 4. Chapter 5 ends the paper with some conclusions and insights.

CHAPTER 2
LITERATURE REVIEW

In this chapter, a literature review of relevant research is provided. It starts off by discussing an area of research that has many similarities to traffic oscillations research, research on the supply chain bullwhip effect. The bullwhip effect in supply chains closely parallels the oscillations seen in congested traffic. Both areas of research heavily rely on control theory, and many useful methods can be adapted for use in both areas. After discussing research on the bullwhip effect, I move to the main topic of the chapter, an overview of the history of and current state of traffic oscillations research.

2.1. Bullwhip Effect Research

This section gives a brief introduction to research on the bullwhip effect. The bullwhip effect refers to an inventory instability often seen in multi-echelon supply chains. Basically, in multi-echelon supply chains, order fluctuations downstream (e.g., fluctuations in the orders from the retailer directly selling to the customer) tend to be amplified as they move up through the suppliers in the chain. Thus, suppliers who are further upstream, away from the final customer, experience much greater fluctuations in their orders than suppliers downstream. Extensive research has been performed to study this phenomenon, but in this section, I simply highlight some research using theoretical methods, since this research is the most pertinent to traffic oscillations research.

Obviously, researchers are interested in pinpointing the causes of the bullwhip effect, as well as quantifying its growth through the supply chain. Lee et al. (2004) point to four causes: demand signal processing, the rationing game, order batching, and price variations. They argue that these four problems lead to information distortion in the supply chain; order fluctuations then naturally result from the distortion of the information.

Chen et al. (2000) quantify the bullwhip effect in a simple two-stage supply chain with demand forecasting and order lead time. This model shows that the variability increases with lead time and can be largely affected by the demand forecasting. To help combat the bullwhip

effect, they suggest centralizing demand information and using smooth demand forecasts that utilize multiple observations when estimating future demand.

There have been many other research efforts to find strategies to help reduce or eliminate the bullwhip effect and to quantify their effects. For example, Ouyang (2007) analyzes the effect of sharing customer demand information with upstream suppliers and shows that the bullwhip effect can be reduced, although not completely eliminated, by sharing customer demand. He measures the bullwhip effect by comparing the variations of orders, as specified by the inventory policy of the suppliers.

Sari (2008) acknowledges the reality, however, that the downstream suppliers who directly deal with the customer do not have much incentive to share this information; several different partnership programs have been developed to offer incentives to share information. Sari uses simulation to show the benefits of two such programs, vendor-managed inventory (VMI) and collaborative planning, forecasting and replenishment (CPFR), by comparing them to a traditional supply chain. He shows that both programs show benefits, but CPFR is more robust and provides a larger benefit.

Obviously, some of the strategies and models used for supply chains are not directly transferable to the study of traffic oscillations. Nevertheless, insights into traffic oscillations can be drawn from research on the bullwhip effect. For example, connected vehicles are becoming a big topic in transportation, and this connection could provide opportunities to share information that could help combat traffic oscillations. It could also provide the conditions necessary to centralize decision making, one strategy shown to combat the bullwhip effect. Until then, other strategies can be used; for example, it might be helpful to provide drivers with information about downstream conditions. This extra information could help them make more informed decisions instead of simply reacting to the behavior of the vehicle in front of them.

2.2. Traffic Oscillations Research

In this section, I give an overview of traffic oscillations research. Traffic oscillations research can be divided into three main categories: (i) research using theoretical methods to understand and study the oscillations through models; (ii) research using empirical methods to

observe and study the oscillations through real-world field data; and (iii) research joining theoretical and empirical methods. The following subsections will provide a summary of these three categories of traffic oscillations research.

2.2.1. Theoretical Methods

Traffic oscillations research using theoretical methods dates back to the 1950's. Early on, linear car-following models were used in theoretical research. For example, Chandler et al. (1958) and Herman et al. (1959) use linear car-following models, along with frequency-domain methods, to determine the criteria necessary for stable traffic flow. These linear models yield useful closed-form equations to model the propagation of an oscillation through a platoon. These closed-form equations allow researchers to exactly quantify the theoretical effects of the model parameters on oscillation propagation.

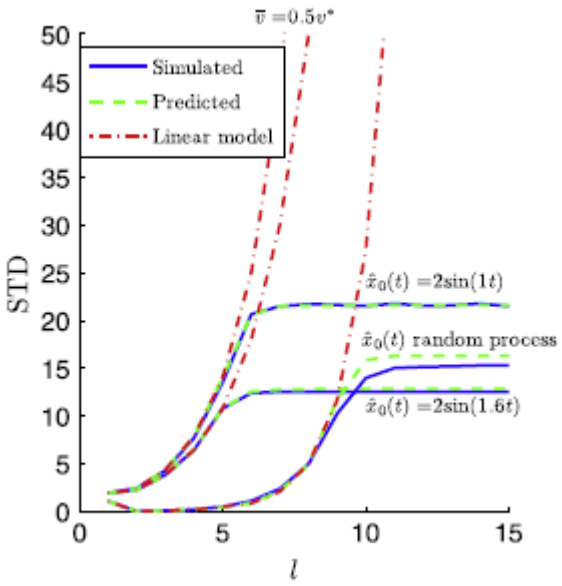

Figure 3: Oscillation propagation using linear and nonlinear models (source: Li and Ouyang, 2011)

Over time, however, it has become apparent that linear models are not realistic when used to model traffic oscillation propagation through a platoon of vehicles. In particular, linear models predict exponential growth of the oscillation amplitude through a platoon (e.g., Herman

et al., 1959). It has been theorized that this inaccuracy is due to the lack of realistic bounds on the operational characteristics of the vehicles and the behavior of the drivers. For example, there is no upper bound on the speed of the vehicle. Obviously in the real world, vehicles have an upper limit on their speed; furthermore, drivers are not likely to feel comfortable or safe when driving at very high speeds.

Thus, nonlinear models were developed to more realistically reproduce driver behavior in congested traffic and to allow better study of the phenomenon (Gazis et al., 1961; Gipps, 1981; Bando et al., 1995). Figure 3 shows the oscillation propagation through a platoon, as it would be calculated using a linear model and a nonlinear model. It should be noted that STD stands for standard deviation; one way that the magnitude of an oscillation is measured is by taking the standard deviation of the oscillatory component of the trajectory. The nonlinear model predicts that the magnitude of the oscillations will plateau, while the linear model predicts unbounded growth through the platoon. It is well-known that the propagation predicted with nonlinear models more closely resembles that seen in the real world.

Newell (1961) proposes a nonlinear car-following model in which the oscillations propagate as in linear theory but the evolution of the oscillations over time and space more realistically reflect that seen in the real world. Treiber et al. (2000) use another nonlinear model, the intelligent driver model, to show that traffic oscillations are often caused by road inhomogeneities, such as lane closures or uphill segments of the road. Laval et al. (2014) use a modified version of Newell's 2002 car-following model to suggest that the discrepancy between the desired and actual acceleration of a vehicle, caused by driver error, can lead to oscillations. These studies show that a small perturbation in the behavior of the leading vehicle can lead to large traffic oscillations upstream.

Unfortunately, nonlinear models are also much more complicated to study, with closed-form analysis being especially difficult. Due to this difficulty, many researchers have had to turn to numerical simulation for their analysis. Recently, however, Li and Ouyang (2011) proposed a describing function approach (DFA) to analytically predict the propagation of the oscillations through a platoon of vehicles.

2.2.2. Empirical Methods

Empirical data is invaluable in providing researchers with the opportunity to observe and study traffic oscillations in the real world. In the beginning, the only empirical data available was loop detector data; consequently, many researchers have developed methods to calculate either the macroscopic or oscillatory properties of the traffic flow, often by aggregating this data. For example, Treiber and Helbing (2002) develop the adaptive smoothing method to find traffic velocity, density, and flow as a function of time and space using loop detector data, giving them a way to visualize the propagation of congestion upstream. Zielke et al. (2008) use the Mauch, cross-correlation, and autocorrelation methods to determine the oscillation amplitude, propagation speed, and frequency from this data. They then use these measurements to compare traffic oscillation characteristics in different countries around the world, pointing out the importance of considering the characteristics of the infrastructure and traffic when developing models to describe this phenomenon.

Other researchers have concentrated on using data to pinpoint possible sources of the oscillations. These studies have led to the identification of some causes such as the large reaction times of drivers. Laval (2011) studies the hysteresis phenomenon in congested traffic and points to driver error as a cause of the traffic oscillations. He claims this error is due to the aggressive and timid behavior of the drivers. Ferrari (1989) also points to driver behavior as a cause of traffic oscillations, but he explains that frequent lane changes by drivers can result in oscillations.

As data collection technologies and techniques have improved over the years, good-quality microscopic trajectory data have become available, allowing for more detailed analysis of traffic oscillations. For example, Neubert et al. (1999) use single-vehicle data to identify new traffic states that exist in congested traffic flow, while Chen et al. (2012) use trajectory data to develop a behavioral car-following model to study the formation and propagation of the oscillatory waves.

Until recently, most empirical methods of studying traffic oscillations have focused on using time-domain analyses. Time-domain analysis of empirical data can run into some problems, though. Oftentimes, there is noise in the field data due to errors in data collection.

Frequency-domain methods, however, are naturally better adapted to separate the noise from the traffic oscillations.

Recent studies have shown, therefore, that frequency-domain methods can more accurately measure the oscillatory characteristics of traffic flow. Li et al. (2010) propose a frequency spectrum analysis to calculate the characteristics of the oscillations, such as the period and magnitude, from loop detector data. They use signal processing techniques to distinguish the oscillations from noise in the data.

Zheng et al. (2011) then propose a wavelet transform method to determine the spatiotemporal properties of traffic oscillations using loop detector data. This method allows them to determine the location of the origin of the oscillation, giving them the opportunity to pinpoint possible causes of the oscillation. Zhao et al. (2014) suggest an extended spectral envelope method to study the evolution of the oscillations and to determine the strength of oscillations at various locations.

2.2.3. Joining Theoretical and Empirical Methods

Clearly, a lot of research has been performed to date developing both theoretical and empirical methods. It would be ideal to be able to calibrate or validate the theoretical models and predictions with empirical data. Therefore, there has been much work focusing on calibrating and validating these models.

For example, Kesting and Treiber (2008) develop a calibration technique that utilizes trajectory data; they use the genetic algorithm and a nonlinear optimization function defined by the absolute and relative errors between a simulated and observed trajectory to perform the calibration on the intelligent driver and velocity difference models. Thus, they focus on reproducing the time-space diagram. Treiber and Kesting (2012) also propose a way to calibrate and validate intelligent driver and human driver models using stationary detector data; they calibrate the car-following model according to driver behavior and then validate it using spatiotemporal measures. Li et al. (2012) turn their focus to frequency-domain characteristics; they expand previous work (Li and Ouyang, 2011) to calibrate Newell's nonlinear car-following

models using trajectory data, with the goal of accurately predicting the growth of the oscillations through the platoon of vehicles.

CHAPTER 3
METHODOLOGY[1]

In this chapter, I propose a new method to calibrate nonlinear car-following laws based on real-world trajectories, taking into account not only driver's car-following behavior but also the vehicle trajectory's time-domain (e.g., location, speed) and frequency-domain properties (e.g., peak oscillation amplitude). I use Newell's 1961 car-following model as an example and calibrate its parameters with a penalty-based maximum likelihood estimation procedure. I then describe a series of experiments performed using NGSIM data to illustrate the proposed technique.

3.1. Methodology

I start this section by describing a general model calibration technique based on velocity and spacing observations. Then, a new feedback mechanism is introduced to improve traffic reproduction accuracy in time- and frequency-domains.

3.1.1. Model Calibration

I consider a set of field trajectories from a platoon of $n + 1$ vehicles in one lane, indexed from downstream to upstream by $i = 0, 1, \ldots, n$. For vehicle i, let $x_i(t)$ be the recorded position at time $t \in T_i$, where T_i is the discrete recorded time set with sampling step length Δt (e.g., T_i = {0s, 0.1s, 0.2s, …}), and $\boldsymbol{x_i} = \{x_i(t)\}_{t \in T_i}$ be the entire trajectory, assumed to be monotonically increasing over t.

For a given pair of consecutive trajectories $\{\boldsymbol{x_{i-1}}, \boldsymbol{x_i}\}$, at time t, the observed velocity $v_i(t)$ of the following vehicle is estimated from data as

[1] Reprinted, with permission, from Rhoades, C., Wang, X., Ouyang, Y. Calibration of nonlinear car-following laws for traffic oscillation prediction. Transportation Research Procedia. In press. Figures 4-6 originally created by Wang, X.

$$v_i(t) \approx \frac{x_i(t+\Delta t) - x_i(t)}{\Delta t}, \tag{1}$$

and the observed spacing by driver *i*, $s_i(t, \tau_i)$, is a time-shift of $x_{i-1}(t) - x_i(t)$, i.e.,

$$s_i(t, \tau_i) = x_{i-1}(t - \tau_i) - x_i(t - \tau_i) \tag{2}$$

assuming a time lag of τ_i, which can, for example, account for reaction time.

For simplicity, I assume each vehicle independently follows a general class of nonlinear car-following law $F(\cdot)$ where the desired velocity of the following vehicles, $v_i^*(t)$, is defined using the spacing between the leading and following vehicles, $s_i(t, \tau_i)$, although the methodology suggested here could be modified to accommodate other types of laws as well. Each nonlinear car-following law can be specified by a parameter set H_i in addition to τ_i; i.e.,

$$v_i^*(t) = v(s_i(t, \tau_i)|H_i). \tag{3}$$

I suppose that each observed velocity comes from the desired velocity plus an error term ε_i, as shown below:

$$v_i(t) = v_i^*(t) + \varepsilon_i = v(s_i(t, \tau_i)|H_i) + \varepsilon_i\ , \tag{4}$$

where the error term ε_i follows a general probability density function $\phi(\cdot\,|\Sigma_i)$ with its parameter set Σ_i.

Given the trajectory data of the whole platoon $\{\boldsymbol{x}_i\}_{i=0}^n$, normally exhibiting congestion, I aim to obtain parameters $\{H_i, \tau_i, \Sigma_i\}_{i=1}^n$, each of which is calibrated based on a pair of consecutive trajectories; e.g., $\{\boldsymbol{x_{i-1}}, \boldsymbol{x_i}\}$. These calibrated parameters should reproduce $\{\boldsymbol{x_i}\}_{i=1}^n$ in both the time-space diagram (with regard to the trajectories) and the frequency domain (with regard to the oscillation amplitudes).

The parameters can be calibrated by maximizing the likelihood function for observing any pair of trajectories $\{\boldsymbol{x_{i-1}}, \boldsymbol{x_i}\}$; i.e.,

$$\boldsymbol{\mathcal{L}}(H_i, \tau_i, \Sigma_i) = \prod_{t \in T_i} \phi(v_i(t) - v(s_i(t, \tau_i)|H_i)|\Sigma_{\mathrm{i}}). \tag{5}$$

For notation convenience, I simply define $M_i = \{H_i, \tau_i\}$ to be the car-following law parameter set. Then, an open-loop calibration of the car-following law can be written as follows.

Maximum Likelihood Estimation (MLE):

$$[M_i^L, \Sigma_i^L] = \underset{M_i, \Sigma_i}{\operatorname{argmax}} \mathcal{L}(M_i, \Sigma_i) \tag{6}$$

Note that M_i^L contains the optimal parameters in the car-following law that will maximize the accuracy of predicting $v_i^*(t)$. This simple method has several limitations, however. First, the maximum likelihood function is highly nonlinear in the parameters, and hence the search for the best parameter values may easily become trapped in local optima. For example, the value of H_i^L would be very sensitive to the value of reaction time τ_i^L, as illustrated by the data plots in Figure 4. Second, the error terms are assumed to be independent; hence the estimation method above does not explicitly address the temporal continuity and autocorrelation of a driver's car-following behavior. Finally, there is no explicit consideration of oscillation properties, and hence the resulting car-following law will be unlikely to accurately reproduce the oscillatory components (which will be illustrated later in our numerical experiments). In the following subsections, I propose to improve the model parameter estimation by explicitly addressing feedbacks from the reproduction of both the time- and frequency-domain traffic components.

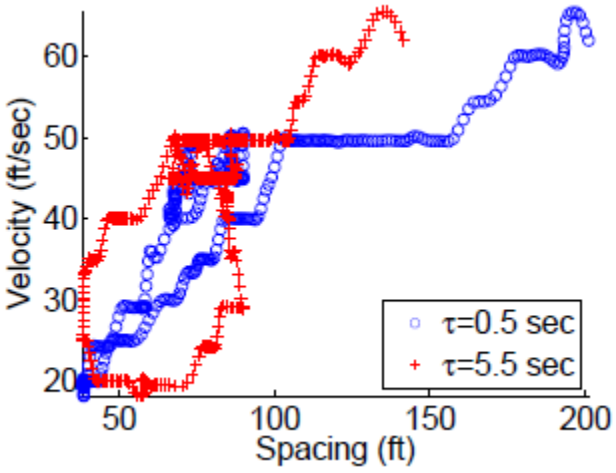

Figure 4: Impact of reaction time on velocity-spacing plot (source: NGSIM data)

3.1.2. Simulation-Based Feedback

In this section, I will first introduce time- and frequency-domain traffic prediction errors. These errors will be used to evaluate any given car-following law M_i and will later be incorporated into the calibration procedure via a penalty method.

3.1.2.1. Time-Domain Feedback

Since almost all field trajectory data are collected in the time domain, verifying M_i in the time domain is intuitive. I only need to reproduce the trajectory of the following vehicle in the time-space diagram and measure the difference from its observed counterpart.

Given a pair of field trajectories $\{\boldsymbol{x_{i-1}}, \boldsymbol{x_i}\}$ that span time ranges T_{i-1} and T_i, respectively, and a car-following model M_i, I simulate the following vehicle's trajectory $\hat{\boldsymbol{x}}_i$ as follows.

For any $t \in T_i$, if $t - \tau_i \notin T_{i-1} \cap T_i$, I have $\hat{x}_i(t) = x_i(t)$. Otherwise,

$$\hat{x}_i(t + \Delta t) = \hat{x}_i(t) + \hat{v}_i(t)\Delta t, \tag{7}$$

where $\hat{v}_i(t) = v(x_{i-1}(t - \tau_i) - \hat{x}_i(t - \tau_i)|H_i)$ is the simulated velocity, as given by the car-following model. It should be noted here that each following vehicle trajectory is reproduced based on its observed (i.e., accurate) leading vehicle trajectory.

Then, I define the time-domain error associated with parameters M_i as

$$e_i^T := \frac{1}{|T_i|}\sqrt{\sum_{t \in T_i}[x_i(t) - \hat{x}_i(t)]^2}\,, \tag{8}$$

where $|T_i|$ is the number of elements in T_i. Obviously, a smaller e_i^T indicates a more accurate reproduction of the time-domain trajectory. This error reflects the accuracy of trajectory reproduction at every time step and hence addresses the continuity and autocorrelation of a driver's car-following decisions.

3.1.2.2. Frequency-Domain Feedback

Most oscillation properties, e.g., amplitude and periodicity of oscillation, can be easily captured by analyzing the oscillation component $x_i^o(t)$ of the vehicle trajectory in the frequency domain, which is defined here as in Li and Ouyang (2011).

First, I transform the time-domain field data into the frequency domain. In field data capturing congested traffic, especially when the "stop-and-go" phenomenon shows periodically in the trajectory, the frequency spectrum of $x_i^o(t)$ normally contains a highly dominant frequency component (Li et al., 2010), i.e., the fundamental frequency, denoted by Ω_i, and hence $x_i^o(t)$ can be approximated by a sinusoid, shifted to zero phase without loss of generality,

$$x_i^o(t) \approx A_i \sin(\Omega_i t), \qquad \forall t \in T_i, \tag{9}$$

where A_i is the oscillation amplitude. Considering that the field data are noisy and may only contain a small number of oscillation periods (e.g., only one stop-and-go cycle), which means the typical discrete Fourier transform is not effective, I use the following wavelet method (Daubechies, 1992) to estimate Ω_i and A_i for vehicle *i*'s trajectory. First, I estimate

$$\Omega_i = \underset{\Omega}{\operatorname{argmax}} \left\{ \max_{t \in T_i} \int_{-\pi/\Omega}^{\pi/\Omega} \psi(u, \Omega) x_i^o(t-u) du \right\}, \tag{10}$$

where

$$\psi(u, \Omega) = \frac{\Omega}{\pi} \sin(\Omega u), \qquad \forall \Omega > 0, u \in \mathbb{R}, \tag{11}$$

is the wavelet function. Let

$$t_i^m = \underset{t \in T_i}{\operatorname{argmax}} \int_{-\pi/\Omega_i}^{\pi/\Omega_i} \psi(u, \Omega_i) x_i^o(t-u) du. \tag{12}$$

Then, the observed oscillation amplitude, A_i, is estimated as

$$A_i = \frac{\Omega_i}{\pi} \int_{t_i^m - \pi/\Omega_i}^{t_i^m + \pi/\Omega_i} e^{-j\Omega_i t} x_i^o(t) dt, \tag{13}$$

where j is the imaginary unit.

I similarly apply the wavelet method described above to the simulated trajectory, denoted by $\hat{A}_i$. Then the frequency-domain error under M_i can be defined using the maximum value on the trajectory's frequency spectrum (i.e., the one dictating the oscillation amplitude) as follows:

$$e_i^F(M_i) := \left|A_i - \hat{A}_i\right|. \tag{14}$$

3.1.3. Model Integration and Solution

The aforementioned MLE model provides a good starting point for finding the optimal parameters for the car-following law, but it can be further improved by incorporating the time- and frequency-domain errors.

First, define

$$\boldsymbol{\mathcal{M}_i}(\gamma^F, \gamma^T) := \{M_i : e_i^F(M_i) \le \gamma^F, e_i^T(M_i) \le \gamma^T\}, i = 1, 2, \dots, n, \tag{15}$$

where $\gamma^F, \gamma^T \in \mathbb{R}_+^2$ are predetermined tolerances for the frequency- and time-domain errors. All parameters in $\boldsymbol{\mathcal{M}_i}(\gamma^F, \gamma^T)$ guarantee acceptable traffic reproduction errors no larger than γ^F and γ^T.

I assume that the model calibration shall be subject to guaranteed reproduction errors, as the following:

$$\max_{M_i \in \boldsymbol{\mathcal{M}_i}(\gamma^F, \gamma^T), \Sigma_i} \boldsymbol{\mathcal{L}}(M_i, \Sigma_i), \qquad \text{if } \boldsymbol{\mathcal{M}_i}(\gamma^F, \gamma^T) \neq \emptyset\,. \tag{16}$$

It is obvious that $|\boldsymbol{\mathcal{M}_i}(\gamma^F, \gamma^T)|$ is non-decreasing over either γ^F or γ^T, and $\boldsymbol{\mathcal{M}_i}(+\infty, +\infty) \neq \emptyset$. Further, if $\boldsymbol{\mathcal{M}_i}(0,0) \neq \emptyset$, then (16) yields the ideal model that perfectly reproduces the field data in both the time and frequency domains. It is difficult, however, to judge if $\boldsymbol{\mathcal{M}_i}(\gamma^F, \gamma^T) \neq \emptyset$ or to choose appropriate γ^F and γ^T from the field data before I solve (16).

To find a proper balance between the time- and frequency-domain errors without explicitly specifying the error thresholds, I propose the following penalty-based optimization (Yenaiy, 2005).

Penalty-based Maximum Likelihood Estimation (pMLE):

$$\lim_{p\to\infty} \max_{M_i,\Sigma_i} \{\log \boldsymbol{\mathcal{L}}(M_i, \Sigma_i) - p[\alpha e_i^T(M_i) + (1-\alpha) e_i^F(M_i)]\}, \tag{17}$$

where $\alpha \in [0,1]$ is a balancing coefficient and p specified the relative weight of the penalties.

The solution to pMLE offers a balance among the likelihood estimator and the errors in both time and frequency domains. When p is small, the objective is near the optimal $\log \boldsymbol{\mathcal{L}}(M_i, \Sigma_i)$, which provides a relatively good initial solution. Then, as p increases, the errors in both domains are reduced significantly, while sacrificing the likelihood. Toward the end of the iteration, when either e_i^F or e_i^T is near its local or global minimum, the increasing p can still guarantee the reduction of the other error. The objective (17) is expected to finally achieve the best value when no further improvement is possible.

To solve pMLE at each iteration, any meta-heuristic search method that allows embedded simulation could be effectively used. I use a genetic algorithm that is terminated when either the number of iterations reaching a set maximum or the fit of the model does not improve over a set number of iterations.

3.2. Describing Function Approach Prediction

In the previous section, frequency-domain feedback is provided via spectrum analysis of the simulated trajectories. An alternative approach could be developed based on analytical predications from Li et al. (2012) so as to reduce computational burden. Given the oscillation properties of the leading vehicle, the DFA can be used to predict those of the following vehicle under a class of nonlinear car-following law M_i that governs the oscillatory components of two adjacent trajectories:

$$x_i^o(t) = \boldsymbol{L_i}[\boldsymbol{N_i}\big(x_{i-1}^o(t) - x_i^o(t)\big)] \tag{18}$$

where $\boldsymbol{L_i}[\cdot]$ is a linear operator with low-pass filter (e.g., integrator) and $\boldsymbol{N_i}(\cdot)$ is a nonlinear function of spacing, in which the output retains the same fundamental frequency as the input.

I reformulate (18) in the frequency domain. Let $X_{i-1}(\Omega)$, $X_{i-1}(\Omega)$, and $\tilde{\boldsymbol{L}}_{\boldsymbol{i}}(\Omega)$ be the Fourier transform of $x_{i-1}^{o}(t)$, $x_{i}^{o}(t)$, and $\boldsymbol{L}_{\boldsymbol{i}}[\cdot]$, respectively, and $S_i(\Omega) := X_{i-1}(\Omega) - X_i(\Omega)$. Taking Fourier transform on both sides of (18) yields

$$X_i(\Omega) \approx \tilde{\boldsymbol{L}}_{\boldsymbol{i}}(\Omega) \cdot \tilde{\boldsymbol{N}}_{\boldsymbol{i}}(|S_i(\Omega)|) \cdot S_i(\Omega), \tag{19}$$

where

$$\tilde{\boldsymbol{N}}_{\boldsymbol{i}}(A) = \frac{2\int_0^{2\pi} N_i(A\sin(t)e^{-jt})dt}{\pi} \tag{20}$$

is the describing function. For example, the block diagram showing this process for Newell's nonlinear car-following law can be seen in Figure 5.

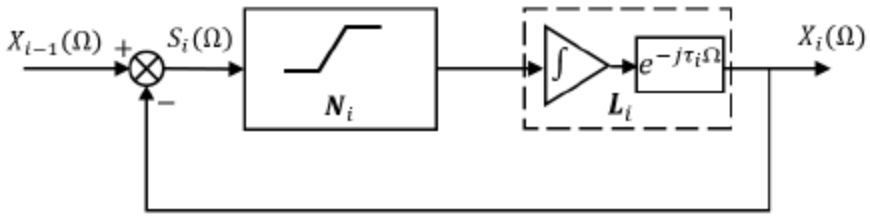

Figure 5: Block diagram for Newell's nonlinear car-following law

Li et al. (2012) proves $|X_i(\Omega)|$ can be predicted by solving the following system of equations,

$$\begin{cases} |X_i(\Omega)| = \left|\tilde{\boldsymbol{L}}_{\boldsymbol{i}}(\Omega) \cdot \tilde{\boldsymbol{N}}_{\boldsymbol{i}}(|S_i(\Omega)|)\right| \cdot |S_i(\Omega)| \\ |X_{i-1}(\Omega)| = \left|1 + \tilde{\boldsymbol{L}}_{\boldsymbol{i}}(\Omega) \cdot \tilde{\boldsymbol{N}}_{\boldsymbol{i}}(|S_i(\Omega)|)\right| \cdot |S_i(\Omega)|. \end{cases} \tag{21}$$

Denote the solution of (21) by

$$|X_i(\Omega)| = \mathrm{DFA}_{\mathrm{M_i}}(|X_{i-1}(\Omega)|, \Omega). \tag{22}$$

Now, I am able to address the oscillation propagation reproduction. I first use the wavelet method described in section 3.1.2.2 to obtain the oscillation properties of the whole platoon, $\{\Omega_i\}_{i=0}^{n}$ and $\{A_i\}_{i=0}^{n}$. I then define the amplification ratio of vehicle i as $R_i = A_{i-1}/A_i$ for $i = 1, 2, \ldots, n$; this ratio is an important factor depicting the oscillation propagation.

Theoretically, $\Omega_{i-1} = \Omega_i$ should always hold due to the assumption of $\boldsymbol{N_i}(\cdot)$. There may, however, exist small gaps between them from the above wavelet method. Here I propose a simple modification: (i) combine trajectories $\{\boldsymbol{x_{i-1}}, \boldsymbol{x_i}\}$ into one single trajectory $\boldsymbol{x_{i-1,i}}$ by shifting the first point of $\boldsymbol{x_i}$ to the last point of $\boldsymbol{x_{i-1}}$ in the time-space diagram; (ii) repeat the above wavelet method to $\boldsymbol{x_{i-1,i}}$ to obtain the fundamental frequency, denoted by $\bar{\Omega}_i$; and (iii) adjust both Ω_{i-1} and Ω_i to $\bar{\Omega}_i$. Note that this modification is conducted for each pair $\{\boldsymbol{x_{i-1}}, \boldsymbol{x_i}\}$ and $\bar{\Omega}_i$ is allowed to vary over i.

Then our task is to estimate $\hat{A}'_i$ based on A_{i-1}, $\bar{\Omega}_i$, and the calibrated parameters M_i. This can be obtained from (22), i.e.,

$$\hat{A}'_i = \mathrm{DFA}_{M_i}(A_{i-1}, \bar{\Omega}_i). \tag{23}$$

This term $\hat{A}'_i$ can be considered as an analytical counterpart of, and can be used to estimate, $\hat{A}_i$ in (14).

3.3. Numerical Example

In this section, empirical trajectory data are used to validate the proposed model calibration and oscillation prediction framework. For illustration, I consider two vehicle platoons from the NGSIM dataset, which was collected from southbound US 101 in Los Angeles, CA from 7:50 - 8:35 AM on June 15, 2005.

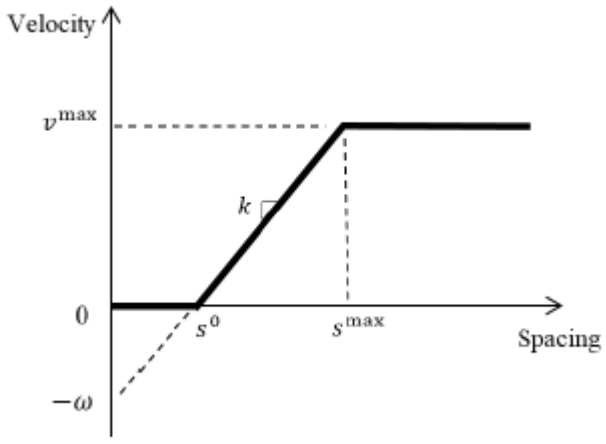

Figure 6: Newell's nonlinear car-following law

I assume that the drivers follow Newell's nonlinear car-following law (Newell, 1961), as shown in Figure 6. The following vehicle i adjusts its desired velocity $v_i^*(t)$ linearly based on the spacing to its leading vehicle $i-1$, subject to physical speed bounds; i.e., in (3) I let

Newell's Model:

$$v_i^*(t) = \text{mid}\{0, k_i[x_{i-1}(t-\tau_i) - x_i(t-\tau_i)] - \omega_i, v_i^{\max}\}, \qquad \forall t \in T_i \tag{24}$$

where ω_i is the backward shockwave speed, k_i is the sensitivity factor of driving aggressiveness, $v_i^{\max}$ is the upper bound on velocity, and again, τ_i is the reaction time. The car-following behavior of vehicle i can be fully specified by $M_i := \{k_i, \tau_i, \omega_i, v_i^{\max}\}$. For convenience, I further define the stopping distance as $s_i^0 := \omega_i/k_i$ and the spacing when desired velocity first reaches the upper bound as $s_i^{\max} := (\omega_i + v_i^{\max})/k_i$.

For most observations, I assume a normal distribution for the error term, with zero mean and standard deviation σ_i, hence I simply have $\Sigma_i = \{\sigma_i\}$. Since drivers do not drive backwards, however, the folded normal distribution is used instead for the case when $v_i^*(t) = 0$. Define $I(\cdot) = 1$ if the expression in $(\cdot)$ is true; or 0 otherwise. Then the likelihood function for a given pair of observed trajectories $\{\boldsymbol{x_{i-1}}, \boldsymbol{x_i}\}$ is given by

$$\begin{aligned}\mathcal{L}(M_i, \sigma_i) = \prod_{t\in T_i} &\left[\frac{1}{\sigma_i}\tilde{\phi}\left(\frac{v_i(t)}{\sigma_i}\right)\right]^{I(v_i^*(t)=0)} \cdot \left[\frac{1}{\sigma_i}\phi\left(\frac{v_i(t) - v_i^{\max}(\mathrm{t})}{\sigma_i}\right)\right]^{I(s_i(t,\tau_i)\geq s_i^{\max})} \\ &\cdot \left[\frac{1}{\sigma_i}\phi\left(\frac{v_i(t) - v_i^*(\mathrm{t})}{\sigma_i}\right)\right]^{I(s_i(t,\tau_i)\geq s_i^{\max})\cdot I(v_i^*(t)=0)},\end{aligned} \tag{25}$$

where $\tilde{\phi}(\cdot)$ and $\phi(\cdot)$ now are the probability density functions of the folded and the normal distribution, respectively.

3.3.1. Case I

I will first illustrate the proposed model calibration technique using a platoon consisting of Vehicles 81 to 93 in the NGSIM data. I set $\alpha = 0.5$ for each pair of vehicle trajectories and use the genetic algorithm to find the model and probability parameters; the calibrated parameters are listed in Table 1.

In Table 1, column "$-\log \mathcal{L}$" indicates the negative log likelihood at convergence, while e^F and e^T respectively indicate the residual frequency- and time-domain errors. Rows "Avg." and "CV" show the mean and coefficient of variation (i.e., the standard deviation divided by the mean) of the entire platoon, respectively. Table 2 shows the minimum, maximum, and average frequency- and time-domain errors for 10 runs of the genetic algorithm. I observe that the majority of the parameters have reasonable values, although there is obvious heterogeneity across the drivers. The frequency-domain errors are much smaller than the time-domain errors for most vehicles, implying far better reproduction in the frequency domain. Towards the end of the iterative calibration algorithm, it is often observed that the time-domain error will remain relatively stable, while the frequency-domain error continues to decrease to an infinitesimal value.

Table 1: Calibration results for Case I

Vehicle	k (1/sec)	τ (sec)	ω (ft/s)	$v^{\max}$(ft/s)	σ	$-\log \mathcal{L}$	e^F	e^T
82	0.65	1.32	0.78	71.54	4.24	2.67	7.28e-6	0.30
83	0.74	2.07	2.00	67.94	6.27	3.09	8.84e-6	0.76
84	0.49	1.67	-0.86	51.85	2.95	3.67	1.28e-6	0.54
85	0.54	1.52	6.37	77.95	7.32	3.43	2.86e-6	0.76
86	0.47	1.82	1.54	62.73	6.09	3.27	1.95e-6	0.95
87	0.91	0.92	2.75	84.31	4.37	2.83	1.67e-5	0.24
88	0.38	1.02	-0.64	64.08	4.01	2.49	1.86e-5	0.26
89	0.63	2.02	3.05	61.97	6.94	3.67	2.15e-5	0.89
90	0.56	2.45	0.97	65.86	7.79	3.28	6.70e-5	0.92
91	0.41	2.67	0.31	59.00	4.92	4.56	0.033	1.56
92	0.64	1.02	0.78	85.62	4.97	3.03	0.033	0.37
93	0.42	0.42	-5.05	60.88	5.71	3.11	0.031	0.75
Avg.	0.57	1.58	0.99	67.80	5.46	3.26	0.0027	0.69
CV	0.26	0.42	2.71	0.15	0.26	0.16	3.45	0.54

Figure 7 offers a closer look at the velocity-spacing diagrams of Vehicles 88 and 92, as examples. For Vehicle 88, the observed data are distributed across the linear and truncation segments of the Newell's model. The observed data for Vehicle 92 are more clustered within the linear segment – in this case, the parameter value $v^{\max}$ seems to have little effect on the time-domain reproduction, as will be seen later in the sensitivity analysis.

Table 2: Minimum, maximum, and average errors for Case I

Vehicle	Min. e^F	Max. e^F	Avg. e^F	Min. e^T	Max. e^T	Avg. e^T
82	3.48e-8	9.98e-6	4.00e-6	0.300	0.657	0.379
83	2.36e-8	3.24e-6	7.75e-7	0.652	1.406	0.770
84	2.59e-7	7.45e-5	1.09e-5	0.553	1.514	0.876
85	8.29e-8	2.95e-4	3.48e-5	0.761	1.154	0.881
86	7.75e-10	3.32e-5	8.12e-6	0.907	1.065	0.970
87	4.13e-8	3.75e-6	9.62e-7	0.221	0.313	0.241
88	2.23e-7	1.14e-4	2.78e-5	0.246	0.740	0.356
89	2.33e-7	3.27e-6	9.16e-7	0.888	1.031	0.950
90	4.94e-8	2.19e-5	3.76e-6	0.832	1.808	1.106
91	2.13e-9	3.42e-2	1.02e-2	1.419	2.243	1.819
92	6.68e-8	3.85e-5	9.58e-6	0.354	0.518	0.401
93	4.94e-8	2.19e-5	3.76e-6	0.832	1.808	1.106

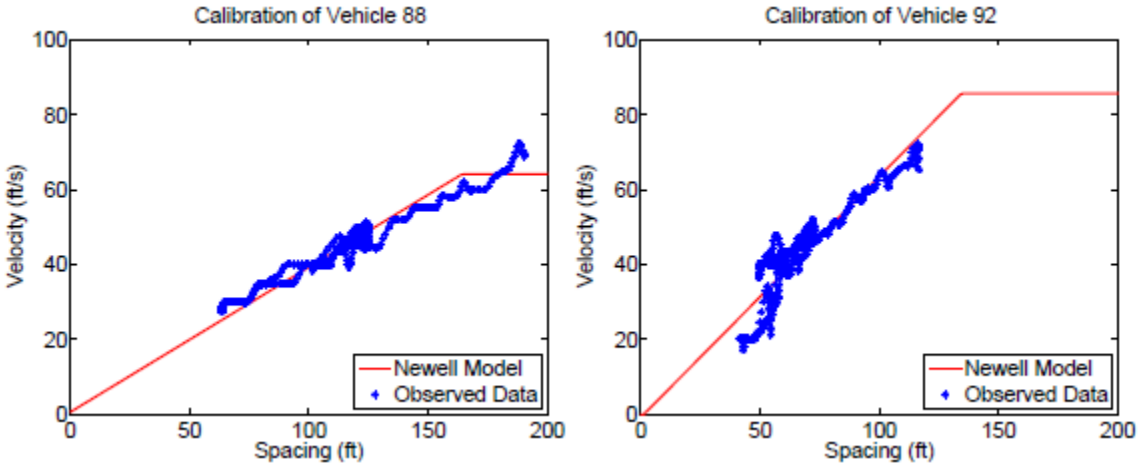

Figure 7: Velocity-spacing diagrams for calibrated Newell's models

Figure 8 illustrates the reproduction of the field data based on the calibrated car-following models. For the time domain, Figure 8(a) shows that the field and simulated trajectories match very well for the whole platoon. Meanwhile, for the frequency domain, Figure 8(b) shows the reproduced oscillation propagation as indicated by, A_i, the cumulative amplitude growth from the first vehicle (#81), and R_i, the pair-wise amplitude growth. The reproduction in the frequency domain is shown using both the simulation-based method (based on $\hat{A}_i$ in section 3.1.2.2) and the DFA (based on $\hat{A}_i'$ in section 3.2), for comparison. I observe that they both

match their corresponding field measurements very well, which simultaneously validates both the analytical prediction and the simulation in the frequency domain.

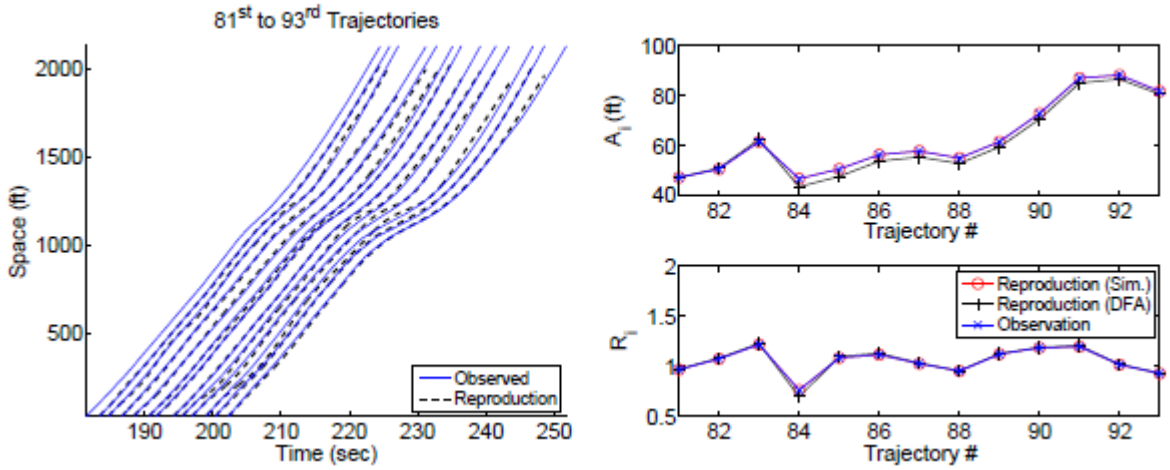

(a) (b)

Figure 8: Reproduction result for Case I (a) Time-space diagram (b) Oscillation propagation

3.3.2. Case II

I next repeat the same calibration procedure for another platoon consisting of Vehicles 311 to 320 from the same NGSIM data – note that now there are two oscillating cycles in the data. The calibrated parameters for the entire platoon are listed in Table 3. It can be seen that, as in Case I, most parameter values seem reasonable, heterogeneity seems to exist across drivers, and the frequency-domain errors are extremely small.

Table 3: Calibration results for Case II

Vehicle	k (1/sec)	τ (sec)	ω (ft/s)	$v^{\max}$(ft/s)	σ	$-\log \mathcal{L}$	e^F	e^T
312	0.53	0.52	6.93	59.05	8.87	3.29	1.20e-6	0.41
313	0.39	0.52	2.32	55.40	6.17	2.74	1.36e-5	0.29
314	0.56	0.12	0.77	89.85	3.80	3.52	5.78e-6	0.48
315	0.47	0.77	6.12	78.85	8.29	3.67	6.28e-6	0.70
316	0.50	0.41	1.45	44.52	9.90	3.42	5.82e-5	0.48
317	0.44	1.52	9.84	46.95	7.54	3.01	1.11e-5	0.41
318	0.40	0.42	6.16	46.10	5.35	3.02	3.20e-4	0.36
319	0.49	1.11	2.38	42.65	5.09	3.34	2.72e-4	0.49
320	0.42	1.35	1.61	45.89	7.44	3.23	1.17e-4	0.51
Avg.	0.47	0.75	4.17	54.87	6.69	3.25	8.95e-5	0.46
CV	0.12	0.63	0.75	0.31	0.27	0.09	1.37	0.24

Table 4 shows the minimum, maximum, and average time- and frequency-domain errors for 10 runs. Figure 9 again shows that the proposed calibration method yields reasonable results in both the time and frequency domains.

Table 4: Minimum, maximum, and average errors for Case II

Vehicle	Min. e^F	Max. e^F	Avg. e^F	Min. e^T	Max. e^T	Avg. e^T
312	6.51e-8	7.63e-5	1.10e-5	0.399	0.738	0.507
313	1.14e-7	2.23e-4	4.81e-5	0.279	0.625	0.341
314	7.56e-8	2.46e-5	9.69e-6	0.482	1.181	0.599
315	3.24e-8	2.61e-5	7.41e-6	0.686	0.978	0.783
316	1.90e-7	5.68e-5	1.42e-5	0.365	0.639	0.462
317	4.64e-7	5.68e-4	9.93e-5	0.410	0.763	0.550
318	1.90e-6	5.68e-5	1.42e-5	0.365	0.536	0.424
319	5.77e-8	6.11e-5	8.78e-6	0.381	0.562	0.447
320	5.82e-7	2.61e-5	7.56e-6	0.432	0.683	0.506

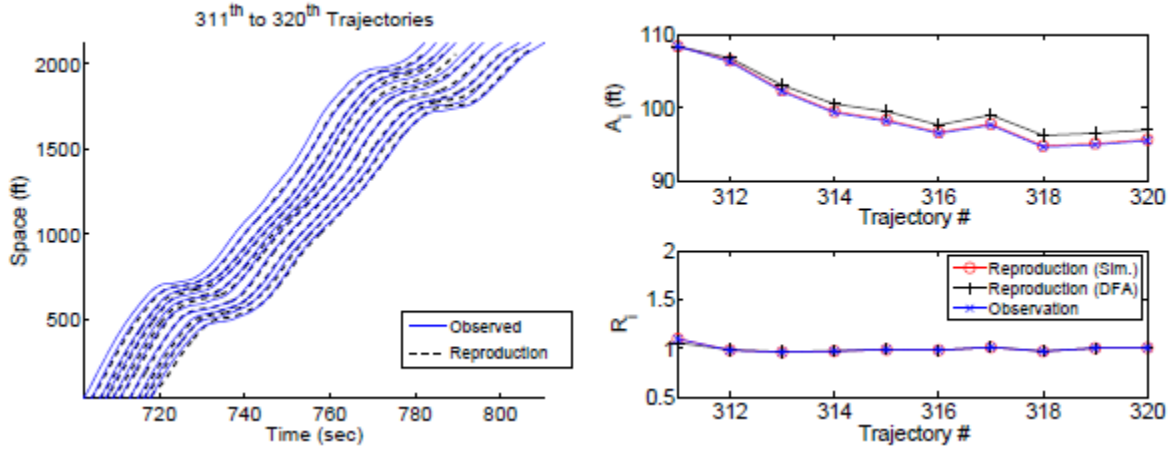

(a) (b)

Figure 9: Reproduction results for Case II (a) Time-space diagram (b) Oscillation propagation

3.3.3. Sensitivity Analysis

Now, I will draw additional insights by conducting a series of sensitivity analyses on the platoon from Case I. First, I evaluate how the value of α (i.e., relative weights of time- and frequency-domain error feedback) affects the calibration results from (17). I compare three scenarios: (i) $\alpha = 1$ (i.e., the frequency-domain penalties are not considered), (ii) $\alpha = 0$ (i.e., the

time-domain penalties are not considered), and (iii) $p = 0$ (i.e., both time- and frequency-domain penalties are not considered).

Figures 10-12 show the reproduction of traffic based on calibration results for each of the three scenarios. It can clearly be observed that when $\alpha = 1$, the reproduction of oscillation propagation in Figure 10(b) is much worse than that in Figure 8(b). On the contrary, when $\alpha = 0$, the reproduction of time-domain trajectories in Figure 11(a) becomes worse than that in Figure 8(a). Note that some simulated vehicle trajectories even contain artificial oscillations due to the lack of control of time-domain properties. In addition, when neither time- nor frequency-domain errors are considered, the reproductions in both domains are much worse than those in Scenarios (i) and (ii).

Second, I explore how sensitive time- and frequency-domain errors are to each model parameter near optimum. This test indirectly reports efficiency of the parameter estimators. For each vehicle, I recalculate e_i^F and e_i^T when k_i, τ_i, ω_i, $v_i^{\max}$, and σ_i are set, one at a time, to be either 10% larger or 10% smaller than their calibrated values in Case I. The results are summarized in Table 5.

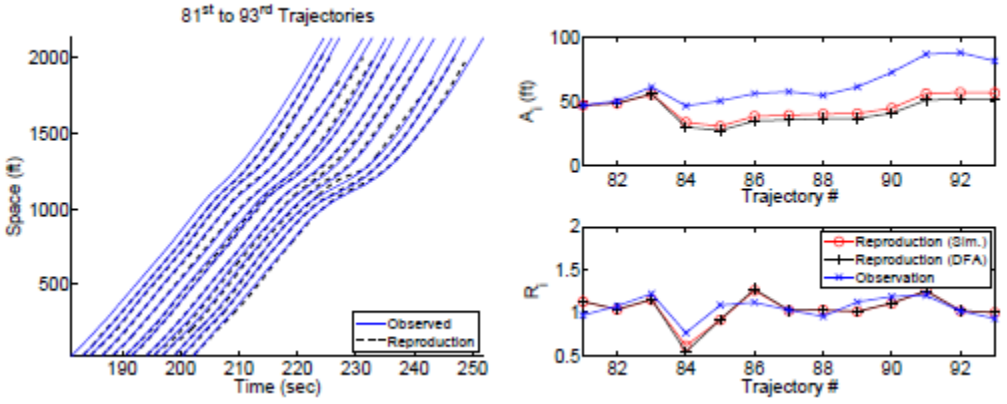

(a) (b)

Figure 10: Reproduction result with $\alpha = 1$ (a) Time-space diagram (b) Oscillation propagation

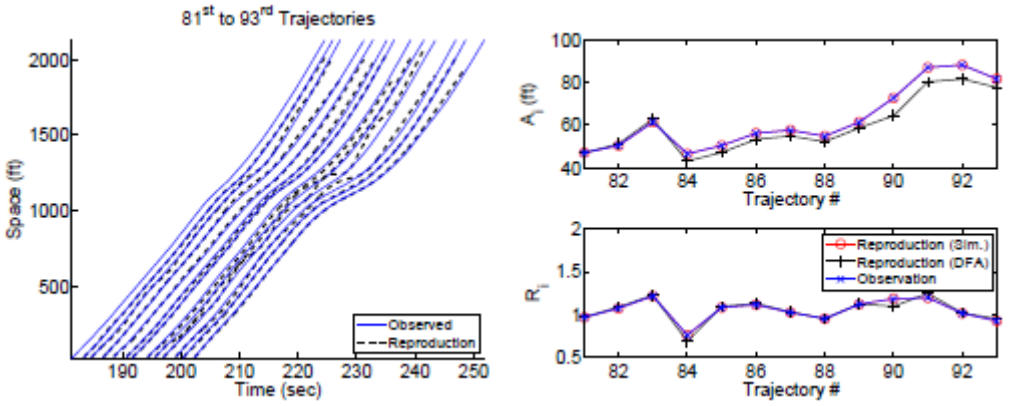

(a) (b)

Figure 11: Reproduction result with $\alpha = 0$ (a) Time-space diagram (b) Oscillation propagation

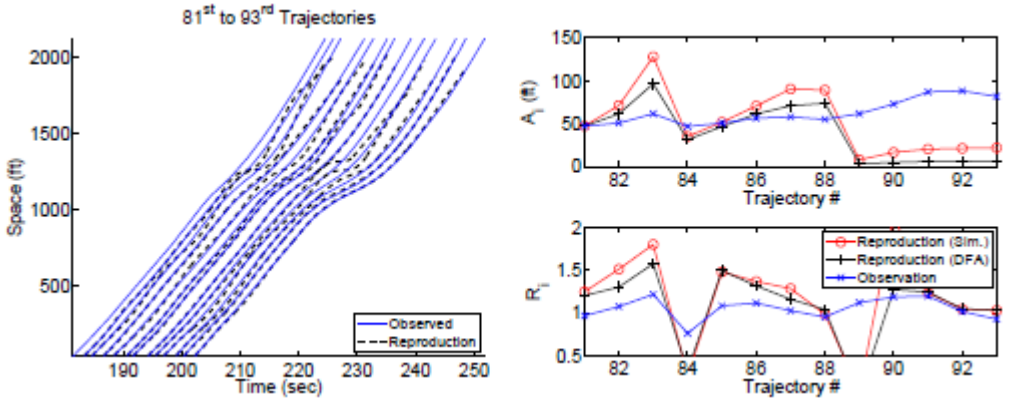

(a) (b)

Figure 12: Reproduction result with $p = 0$ (a) Time-space diagram (b) Oscillation propagation

Several trends can be seen here. First, the absolute changes of e^F are greater than that of e^T when any of k, τ, and $v^{\max}$ varies. On the contrary, the variation of ω only affects e^T, and the variation of σ has no effect on either e^F or e^T. These results imply that k, τ, and $v^{\max}$ jointly determine the oscillatory properties of vehicle trajectories, while the time-domain trajectory properties depend also on ω. In addition, no matter if k increases or decreases, both e^F and e^T increase by a relatively large amount, implying that k is a critical factor that significantly affects traffic oscillation reproduction in both the time and frequency domains.

Table 5: Sensitivity of reproduction errors to model parameters near optimum (e.g., (0.2, -0.1) indicates $e^F \uparrow 0.2$ but $e^T \downarrow 0.1$)

Veh.	$k \uparrow 10\%$	$k \downarrow 10\%$	$\tau \uparrow 10\%$	$\tau \downarrow 10\%$	$\omega \uparrow 10\%$	$\omega \downarrow 10\%$	$v^{\max} \uparrow 10\%$	$v^{\max} \downarrow 10\%$	$\sigma \uparrow 10\%$	$\sigma \downarrow 10\%$
82	(0.76, 0.14)	(1.14, 0.25)	(1.84, 0.011)	(1.06, -0.0033)	(0, 0.00050)	(0, -0.00038)	(0.17, 0)	(10.63, 0.0052)	(0, 0)	(0, 0)
83	(2.68, 0.15)	(0.76, 0.0038)	(8.72, -0.020)	(3.15, -0.048)	(0, 0.00021)	(0, 0,00021)	(0.21, 0.13)	(12.97, -0.14)	(0, 0)	(0, 0)
84	(1.29, 0.13)	(0.93, 0.19)	(3.48, 0.0027)	(1.85, 0.011)	(0, 0.00025)	(0, -000.10)	(16.80, 0.33)	(36.23, 0.35)	(0, 0)	(0, 0)
85	(1.70, 0.08)	(1.52, 0.20)	(5.13, 0.037)	(3.15, -0.016)	(0, 0.0022)	(0, 0.0022)	(18.19, 0)	(39.22, 0)	(0, 0)	(0, 0)
86	(2.26, 0.16)	(2.36, 0.097)	(7.93, -0.013)	(4.83, 0.016)	(0, 0.00014)	(0, 0.00014)	(20.26, 0.0056)	(43.69, -0.098)	(0, 0)	(0, 0)
87	(2.41, 0.11)	(2.58, 0.13)	(8.67, 0.0035)	(5.17, -0.0012)	(0, 0.00045)	(0, 0.00044)	(20.77, 0)	(44.79, 0)	(0, 0)	(0, 0)
88	(3.55, 0.36)	(3.99, 0.35)	(9.76, -0.013)	(5.68, 0.014)	(0, 0.00083)	(0, -0.00060)	(19.77, 0.018)	(42.62, -0.0090)	(0, 0)	(0, 0)
89	(3.72, 0.07)	(4.31, 0.076)	(12.81, 0.053)	(7.45, -0.017)	(0, -0.00015)	(0, 0.00084)	(22.12, 0.053)	(47.70, 0.014)	(0, 0)	(0, 0)
90	(3.84, 0.09)	(4.68, 0.095)	(17.89, 0.18)	(10.71, -0.060)	(0, 6.45e-5)	(0, 2.47e-5)	(26.20, -2.29e-5)	(56.48, -0.099)	(0, 0)	(0, 0)
91	(4.28, 0.08)	(5.71, 0.12)	(24.32, -0.092)	(15.32, 0.091)	(0, 0.00067)	(0, -0.00066)	(31.20, 0.35)	(67.47, -0.24)	(0, 0)	(0, 0)
92	(4.68, 0.07)	(6.27, 0.17)	(25.95, 0.0031)	(16.08, -0.0021)	(0, 0.00042)	(0, 4.17e-5)	(31.63, 0)	(68.41, 0)	(0, 0)	(0, 0)
93	(5.67, 0.10)	(7.34, 0.084)	(23.39, -0.0086)	(14.89, 0)	(0, 0.0028)	(0, 0.00097)	(29.30, 0.074)	(63.36, -0.18)	(0, 0)	(0, 0)

Finally, I conduct a parsimony test on the model parameters to see if some of them can share the same values across the entire platoon, without significantly increasing the calibration errors. It is straightforward that σ could be set to the same value across drivers, based on the sensitivity results in Table 5 above. Noting that k and $v^{\max}$ have relatively small CV (see the last row in Table 1), I assume they are also likely to be the same across drivers. Let $\bar{\sigma}$, $\bar{k}$, and $\bar{v}^{\max}$ be the mean values of σ_i, k_i, and $v_i^{\max}$ across the entire platoon, respectively. Then, I repeat the calibration on Case I using fixed values of $k_i = \bar{k}$, $\sigma_i = \bar{\sigma}$, and $v_i^{\max} = \bar{v}^{\max}$ for all i, and only calibrate τ_i and ω_i. The results are listed in Table 6, and the reproduction of traffic properties is shown in Figure 13.

This result shows that it is fairly reasonable to restrict σ, k, and $v^{\max}$ to be the same across drivers in this platoon. This restriction leads to slightly larger errors in the time and frequency domains, as expected due to the reduced degrees of freedom, but the calibrated model still performs reasonably well.

Table 6: Calibration results of parsimony analysis

Vehicle	k (1/sec)	τ (sec)	ω (ft/s)	$v^{\max}$(ft/s)	σ	$-\log \mathcal{L}$	e^F	e^T
82	0.57	1.35	-1.11	67.81	5.47	3.07	0.07	0.49
83		1.94	-7.98			2.94	0.01	0.56
84		0.12	8.21			3.97	10.3	1.81
85		0.12	10.2			3.68	0.74	0.58
86		1.67	9.17			3.67	0.13	1.13
87		1.12	-15.7			2.83	0.02	0.35
88		0.48	20.92			3.29	0.14	0.65
89		1.95	-0.45			3.99	0.02	0.90
90		2.45	1.77			3.49	0.14	0.93
91		2.74	12.57			5.13	0.49	2.28
92		1.49	-1.53			3.14	0.03	0.49
93		0.13	-5.81			3.63	1.48	1.01

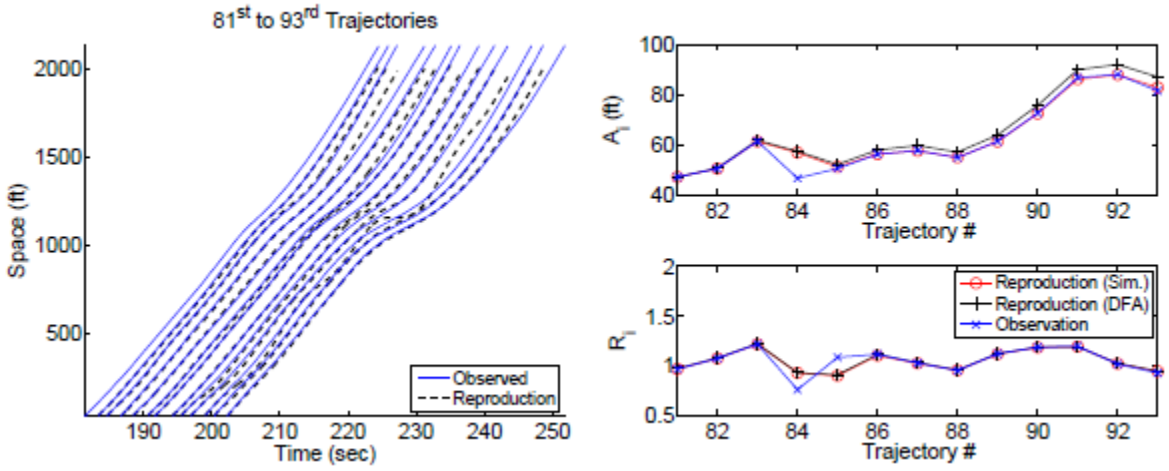

Figure 13: Reproduction result under parsimony (a) Time-space diagram (b) Oscillation propagation

CHAPTER 4
DISCUSSION

In this chapter, I discuss some analyses that were performed to further investigate traffic oscillations. After determining that the calibrated parameters can reproduce traffic oscillations from field data at an acceptable level of accuracy, I can consider possible traffic control strategies that could help to mitigate the oscillations and their negative effects. While considering these potential strategies, I continue to work under the assumption that Newell's nonlinear car-following law can be used to adequately describe the behavior of the drivers. I then use simulation to show the effects of the strategies.

4.1. Calibrated Model Parameters

It would be ideal to be able to use the calibrated model parameters from field data for simulations, since the simulation parameters are then more likely to reflect those typically seen in the real world. In particular, I would like to use the model parameters for Vehicles 82 to 93, the platoon from Case I.

4.1.1. Simulation Difficulty

It should be remembered that in order to calibrate models for an entire platoon, model calibration is performed sequentially on each vehicle using a pair of field trajectory data. If the platoon is then simulated using different boundary conditions, such as the field trajectory data for the first vehicle of the platoon and then only the starting locations of the rest of the platoon, then it is expected that trajectories simulated with the calibrated model parameters will show larger errors, with these errors accumulating through the platoon (Rhoades et al., In press). Indeed, simulating the trajectories with the calibrated model parameters and the aforementioned boundary conditions, set using the field data to provide the initial conditions, results in simulated trajectories that collide. In my simulations, I would like to use the calibrated model parameters but not the initial conditions of the field data, so I define the trajectory of the leading vehicle and

the starting locations of the following vehicles. Nevertheless, different leading trajectories, covering a range of reasonable values for oscillation properties, still result in collisions; Figure 14 shows an example simulation with collisions.

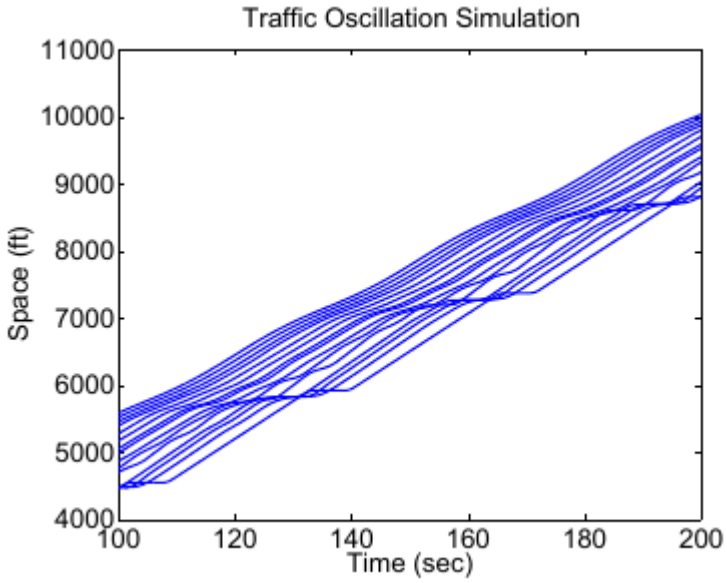

Figure 14: Traffic oscillations simulation experiencing collisions

Therefore, it is clear that the model parameters would have to be adjusted before they could be used. One possible solution to this problem is performing the model calibration for the entire platoon at one time using the aforementioned boundary conditions, with the time-domain error accounting for using reproduced leading trajectories as input instead of field trajectory data (Rhoades et al., In press).

Unfortunately, the NGSIM data collection zone is not long enough to be useful for this purpose. The calibration technique proposed requires time-domain feedback based on the simulated trajectories, but the trajectories can only be simulated where position information is available for both the leading and the following vehicle (i.e., where observed spacing can be calculated). Hence, the simulated trajectory is cut off when the leading vehicle leaves the data collection zone, and it is shorter than the actual field trajectory. If the calibration is not performed sequentially, then all of the simulated trajectories must stop when the first vehicle leaves the data collection zone. Due to the short data collection zone used to collect the NGSIM data, the simulated trajectories are very short by the end of the platoon and stop right before the

field trajectories start oscillating, as seen in Figure 15. The algorithm is still trying to accurately simulate the oscillation propagation through the platoon, though, which leads to large inaccuracies in the time-space diagram as the calibration forces the shortened trajectories to oscillate with amplitudes close to the observed amplitudes. Obviously, a different approach is needed.

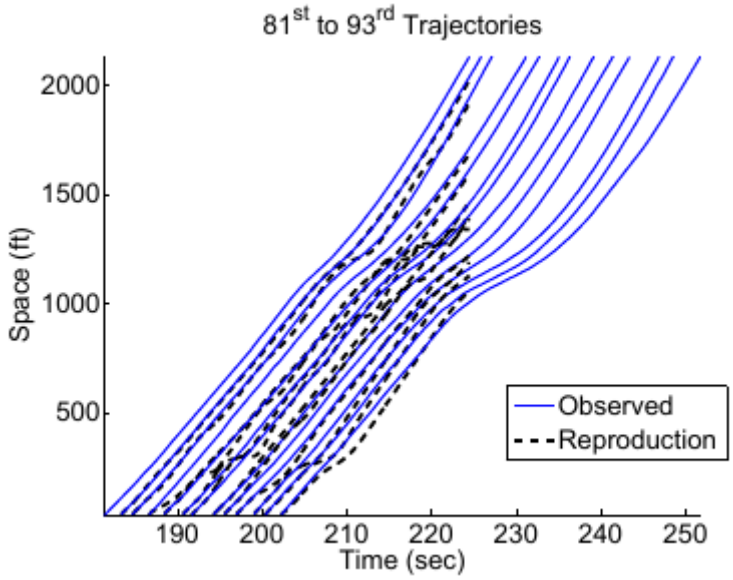

Figure 15: Time-space diagram for non-sequential calibration

4.1.2. Reaction Time

It is noted that the trajectories experiencing collisions in the simulations correspond to the vehicles with large reaction times. Indeed, it can be seen that some of the calibrated reaction times of drivers from Case I are relatively large, while others are smaller. As mentioned in section 3.1.1, the optimization is highly nonlinear and sensitive with respect to reaction time. It is therefore possible that the model calibration becomes stuck in a local optimum with a large reaction time when the global optimum actually corresponds to a different set of model parameters with a smaller reaction time.

The calibration can be modified to avoid this potential problem and further investigate the relationship between the reaction times and the value of the optimization function. I take the reaction time parameter out of the search, incrementing it manually in 0.1 second steps and

performing the calibration for each value. The final values of the optimization function for each reaction time are then compared to choose the model parameters. Table 7 shows the best reaction times and errors from running this process three times, and it compares these values with those from Case I. It can be seen that the reaction times are actually larger overall, but they are also more consistent. The errors are comparable. One possible explanation is that drivers in congestion, especially heavy congestion, do not react as quickly to the vehicle in front of them; they may hesitate before accelerating or decelerating if they think that conditions are likely to change again soon.

Table 7: Reaction time comparison

Vehicle	Case I			Modified Calibration		
	τ (sec)	e^F	e^T	τ (sec)	e^F	e^T
82	1.32	7.28e-6	0.30	1.70	5.64e-5	0.41
83	2.07	8.84e-6	0.76	2.00	5.39e-7	0.62
84	1.67	1.28e-6	0.54	2.20	3.00e-6	0.52
85	1.52	2.86e-6	0.76	2.10	5.79e-6	0.87
86	1.82	1.95e-6	0.95	2.50	1.56e-5	1.04
87	0.92	1.67e-5	0.24	2.20	5.31e-6	0.45
88	1.02	1.86e-5	0.26	2.10	4.08e-6	0.40
89	2.02	2.15e-5	0.89	2.10	3.01e-7	0.84
90	2.45	6.70e-5	0.92	2.30	6.09e-7	0.84
91	2.67	0.033	1.56	1.60	1.99e-7	1.70
92	1.02	0.033	0.37	1.20	0.030	0.38
93	0.42	0.031	0.75	2.50	5.68e-7	0.45

These calibrations give me the best optimization function values for different reaction times, providing me with the data needed to examine this relationship. Figure 16 is a plot of reaction time, as manually incremented, and the optimization function value that is achieved with the given reaction time for Vehicle 82. It should be noted that the values of pMLE shown in the graph are calculated using $p = 1$ to allow for comparison between different values of τ. It can be seen that, as previously mentioned, the relationship between the optimization function and the reaction time is highly nonlinear. Very similar values of pMLE are achieved with very different values of τ, but two very similar values of τ can also result in very different values of pMLE.

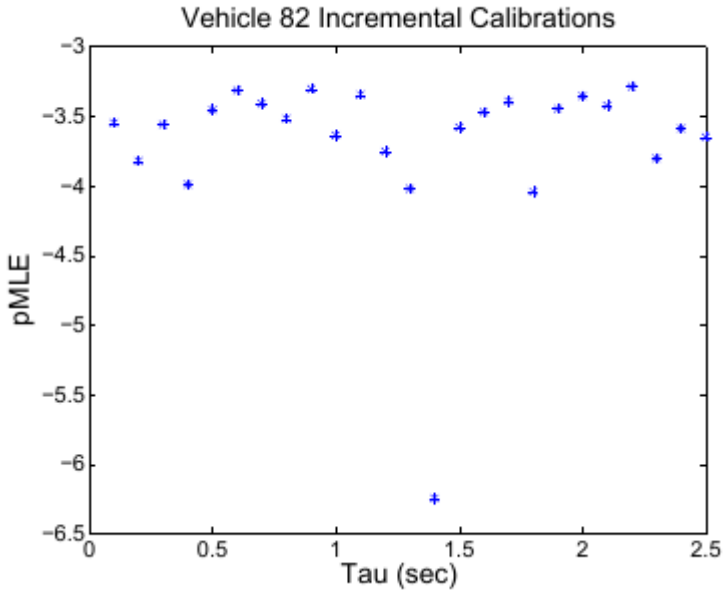

Figure 16: Relationship between tau and pMLE for Vehicle 82

4.1.3. Backward Shockwave Speed

Another possible explanation for the collisions in the simulated trajectories is that the stopping distance, s_i^0, is too small. Quick calculations show that all of the stopping distances from Case I are smaller than 12 feet, with almost all of these values even being smaller than 5 feet. Since stopping distance is the distance between the same point on two consecutive vehicles (e.g., the front bumper) and since vehicles are more than 5 feet long, these values are not reasonable.

In order to further investigate this situation, I manually increase the backward shockwave speed, ω_i, for each vehicle, which also increases the stopping distance. While this helps to improve the situation, there are still collisions. Figure 17 shows that increasing the backward shockwave speed, even beyond practical values, does not completely solve the problem.

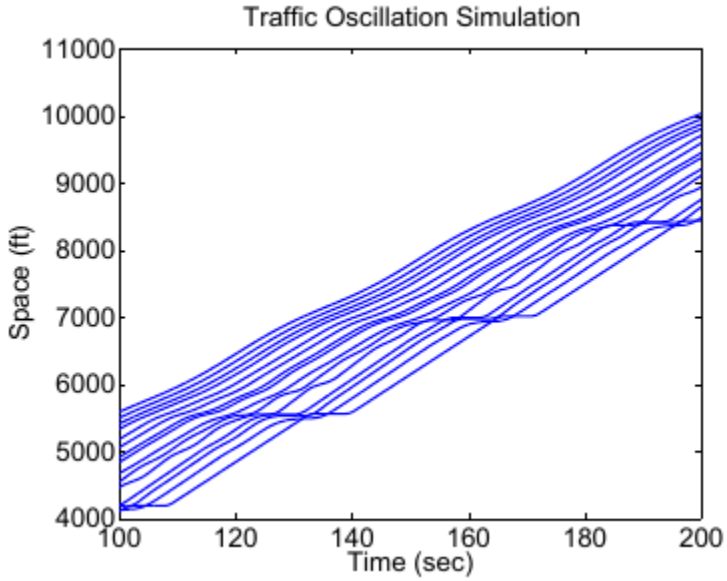

Figure 17: Traffic oscillation simulation with increased stopping distance

4.2. Potential Traffic Control Strategies

At this point, it seems apparent that the model parameters from sequential calibration will not be useful in performing the simulations. Nevertheless, the effect of the parameters on traffic oscillations can still be analyzed to help identify potential traffic control strategies that will help mitigate oscillations. In this section, I discuss studies performed to evaluate these effects and describe several changes in model parameters that help reduce the amplitude of oscillations; then, I suggest several ways to achieve these changes.

4.2.1. Model Parameters and Oscillations

There are two different ways to analyze the effect of the model parameters on oscillations: (i) the describing function approach, as described in section 3.2, and (ii) simulation.

4.2.1.1. Describing Function Approach

One way to study the effect of the model parameters on oscillations is to use the describing function approach. The equations used in this approach are very complicated functions of the model parameters, which makes it almost impossible to derive useful closed-form equations quantifying the relationships between the amplitude of the oscillations and the individual model parameters. Nevertheless, the describing function approach is still a useful way to theoretically predict the effect of changing model parameters on the propagation of traffic oscillations through the platoon. The predicted oscillation propagation through the platoon with the specified model parameters can be compared to the propagation with the changes. In this way, the effect can be predicted.

4.2.1.2. Simulation

Another way to study the effect of the model parameters on oscillations is to use simulation. For this approach, the trajectories are simulated using the car-following law, and the amplitudes are directly measured. Then, the simulation is performed again with the changed parameters, and the results are compared. The results of the DFA and simulation approaches can also be compared to validate the results.

Table 8: Effect of changing model parameters on oscillation amplitude

Case	k (1/sec)	τ (sec)	$v^{\max}$ (ft)	Amplitude (ft)
Base	0.65	1.32	71.54	48.09
1 – increase k	0.78	1.32	71.54	49.82
2 – decrease k	0.52	1.32	71.54	46.70
3 – increase τ	0.65	1.58	71.54	48.97
4 – decrease τ	0.65	1.06	71.54	47.82
5 – increase $v^{\max}$	0.65	1.32	85.85	48.09
6 – decrease $v^{\max}$	0.65	1.32	57.23	39.49
7 – increase k, decrease $v^{\max}$	1.32	1.32	57.23	40.16

4.2.1.3. Analysis Results

It should be recalled from section 3.3.3 that k, τ, and $v^{\max}$ are mainly responsible for determining the oscillatory characteristics of the vehicle trajectories; I am therefore particularly interested in the potential results of changing k, $v^{\max}$, and τ. To investigate, I focus on one vehicle, Vehicle 82, and then I increase and decrease its calibrated k, $v^{\max}$, and τ values by 20%. Still using the trajectory of Vehicle 81 and the starting location of Vehicle 82 as input, I perform a simulation and calculate the magnitude of the oscillation amplitude for Vehicle 82. Table 8 shows the effect of changing k, $v^{\max}$, and τ on oscillation amplitude and indicates that k and τ both have a direct relationship with amplitude. k has a larger impact on amplitude than τ, but both variables have a very small impact on amplitude. The relationship between $v^{\max}$ and amplitude is a little more complicated. Table 8 shows that increasing $v^{\max}$ has no effect on amplitude, which may indicate that the driver never reached a speed of $v^{\max}$ in the simulation. Decreasing $v^{\max}$, however, results in a large reduction in amplitude.

Based on these analyses, it seems that there are several model parameter changes that could produce the desired results. Decreasing k, decreasing $v^{\max}$, and decreasing τ all show potential to decrease the amplitude of traffic oscillations. I will now discuss possible ways to produce these changes in driver behavior and characteristics.

4.2.2. Traffic Oscillation Mitigation Strategies

I would like to consider various strategies that could help mitigate traffic oscillations. Decreasing the model parameters k, $v^{\max}$, and τ have shown some promise in reducing the amplitude of oscillation for a vehicle, and I would like to suggest some strategies that could be employed to potentially create the desired changes in driver behavior.

4.2.2.1. Variable Speed Limit

One way to reduce the maximum speed of drivers, $v^{\max}$, is to impose a mandatory variable speed limit that changes to reflect traffic conditions. While not all drivers follow the

speed limit exactly, this strategy could still help to slow drivers down and therefore to mitigate the propagation of traffic oscillations through a platoon of vehicles. As traffic enters congested conditions where traffic oscillations are likely to form, the speed limit could decrease to help ensure that traffic flow does not become turbulent.

4.2.2.2. Reduced Reaction Time

It has been suggested that variable speed limits do not actually result in lower speeds on roads but that the observed increase in safety is actually caused by reduced reaction times for drivers, τ, due to an increased vigilance in the area. Therefore, it is also possible that the variable speed limit will simply result in a smaller reaction time, which can still help to mitigate traffic oscillations. If the above hypothesis is true, then it may be equally effective to warn drivers when downstream traffic is congested and heighten their vigilance through a warning that traffic is slowed ahead. Of course, if fully-automated vehicles are achieved, then much smaller reaction times will be seen.

4.2.2.3. Advisory Speed

A related possibility is to provide an advisory speed that recommends a speed to drivers based on traffic conditions. I hypothesize that this strategy will have a different effect on driver behavior as compared to the mandatory variable speed limit. It seems clear that more drivers will choose not to reduce their speed if this reduction is voluntary. For the drivers who choose to follow the advisory speed, though, I think the change in their car-following behavior will be more complicated than a reduced $v^{\max}$, as seen with variable speed limits. Since the drivers are trying to stay at the recommended speed, I hypothesize k will increase.

A larger k indicates a more aggressive driver whose speed in the linear section of the speed-spacing diagram changes rapidly with spacing. Since drivers have been given a recommended speed, they expect traffic to travel at that speed, which means they may drive more aggressively than they normally would and show more reluctance to drive at a slower speed. As a result, k will increase. Hence, there will be a narrower range of spacing for the

linearly increasing section of the speed-spacing diagram, as drivers level off at the advised speed at a smaller spacing than the spacing that would normally result in this speed. Drivers will generally be more aggressive – those traveling at a speed lower than the advised speed will push to get to the recommended speed, which means they will choose a higher speed than normal for their observed spacing, and those traveling at the recommended speed will try to avoid slowing down, which means they will have to slow down rapidly if they cannot avoid it.

In addition, I conjecture there will be another section to the speed-spacing diagram. I do not think that drivers will completely level off at the advised speed, regardless of the spacing in front of them. They are likely to retain their maximum speed, and once spacing gets large enough, they will ignore the advised speed. Once again, I think k in this section will be large as drivers either choose to ignore the advisory speed or choose to return to that speed. The spacing for the maximum speed, $s^{\max}$, is likely to be larger than that without the advisory speed, however, since the curve will temporarily level off at the advisory speed. Figure 18 shows an example of the changes that could occur to the speed-spacing diagram when an advisory speed is provided. The original speed-spacing diagram is shown with the thick black lines, and the modified sections are shown with the thin red lines.

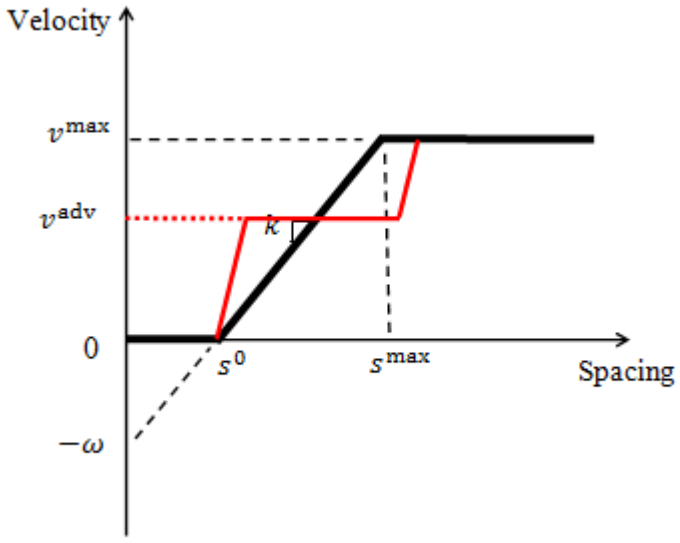

Figure 18: Speed-spacing diagram with advisory speed

These potential changes in the diagram make predicting the effect on traffic oscillations much more difficult, especially if considering the DFA. If I simplify and assume the diagram has the same sections but simply experiences a reduction in $v^{\max}$ to v^{adv} and an increase in k, then it becomes more straight-forward, and it is expected that the amplitude of the oscillations will be reduced. It should be noted that, if the advisory speed limit is implemented well, then drivers should not enter the extra section of the speed-spacing diagram at all, anyway.

CHAPTER 5
CONCLUSIONS

Traffic congestion is a problem that has constantly plagued transportation professionals, and it is not going away anytime soon. Traffic oscillations, a phenomenon often seen in congested traffic, have continued to puzzle transportation researchers, as they continue to search for ways to further understand how these oscillations form and propagate. The model calibration technique proposed in this paper gives researchers the ability to find models to accurately reproduce traffic oscillations from field data in both the time and frequency domains. The ability to reproduce traffic oscillations in turn provides researchers with the opportunity to investigate and analyze the impact of potential traffic control strategies meant to mitigate traffic oscillations and their effects. As ITS technology continues to develop, there will be new ways to provide more information to drivers. This work gives researchers a starting point to determine what information needs to be given to drivers in order to mitigate traffic oscillations.

There are, however, still ways that the current work could be strengthened and expanded. As mentioned, the data used in the numerical examples only cover a short segment of road. Longer trajectory data could allow for non-sequential calibration of the car-following models for the entire platoon; this calibration would provide the ability to reproduce the oscillations using only the trajectory of the first vehicle and the starting locations of the rest of the vehicles in the platoon. Performing the calibration with other field data would also help to further validate the proposed approach. In addition, calibrating and analyzing other nonlinear car-following models could yield more insights into traffic oscillations and how they form and propagate, as well as possible ways to reduce the oscillations.

REFERENCES

Bando, M., Hasebe, K., Nakayama, A., Shibata, A., Sugiyama, Y., 1995. Dynamical model of traffic congestion and numerical simulation. Physical Review E 51 (2), 1035.

Chandler, R. E., Herman, R., Montroll, E. W., 1958. Traffic dynamics: studies in car following. Operations research 6 (2), 165–184.

Chen, D., Laval, J. A., Zheng, Z., Ahn, S., 2012. A behavioral car-following model that captures traffic oscillations. Transportation Research Part B: Methodological, 46 (6), 744-761.

Chen, F., Drezner, Z., Ryan, J., Simchi-Levi, D., 2000. Quantifying the bullwhip effect in a simple supply chain: the impact of forecasting, lead times, and information. Management Science 46(3), 436-443.

Daubechies, I., 1992. Ten lectures on wavelets. Vol. 61. SIAM.

Ferrari, P., 1989. The effect of driver behaviour on motorway reliability. Transportation Research Part B: Methodological 23 (2), 139–150.

Gazis, D. C., Herman, R., Rothery, R. W., 1961. Nonlinear follow-the-leader models of traffic flow. Operations Research 9 (4), 545–567.

Gipps, P. G., 1981. A behavioural car-following model for computer simulation. Transportation Research Part B: Methodological 15 (2), 105–111.

Herman, R., Montroll, E. W., Potts, R. B., Rothery, R. W., 1959. Traffic dynamics: analysis of stability in car following. Operations research 7 (1), 86–106.

Kesting, A., Treiber, M., 2008. Calibrating car-following models by using trajectory data: Methodological study. Transportation Research Record: Journal of the Transportation Research Board 2088 (1), 148–156.

Laval, J. A., 2011. Hysteresis in traffic flow revisited: an improved measurement method. Transportation Research Part B: Methodological 45 (2), 385–391.

Laval, J, Toth, C and Zhou, Y., 2015. A parsimonious model for the formation of oscillations in car-following models. Transportation Research Part B: Methodological 70 (1), 228-238.

Lee, H., Padmanabhan, V., Whang, S., 2004. Information distortion in a supply chain: the bullwhip effect. Management Science 50(12), 1875-1886.

Li, X., Ouyang, Y., 2011. Characterization of traffic oscillation propagation under nonlinear car-following laws. Transportation Research Part B: Methodological 45 (9), 1346–1361.

Li, X., Peng, F., Ouyang, Y., 2010. Measurement and estimation of traffic oscillation properties. Transportation Research Part B: Methodological 44 (1), 1–14.

Li, X., Wang, X., Ouyang, Y., 2012. Prediction and field validation of traffic oscillation propagation under nonlinear car-following laws. Transportation Research Part B: Methodological 46 (3), 409–423.

Neubert, L., Santen, L., Schadschneider, A., Schreckenberg, M., 1999. Single-vehicle data of highway traffic: A statistical analysis. Physical Review E 60 (6), 6480.

Newell, G. F., 1961. Nonlinear effects in the dynamics of car following. Operations Research 9 (2), 209–229.

Ouyang, Y. 2007. The effect of information sharing on supply chain stability and the bullwhip effect. European Journal of Operational Research 182, 1107-1121.

Rhoades, C., Wang, X., Ouyang, Y., Calibration of nonlinear car-following laws for traffic oscillation prediction. Transportation Research Procedia. In press.

Sari, K., 2008. On the benefits of CPFR and VMI: a comparative simulation study. International Journal of Production Economics 113, 575-586.

Schrank, D., Eisele, B., Lomax, T. 2012. TTI's 2012 urban mobility report. Texas A&M Transportation Institute. Texas A&M University System.

Treiber, M., Helbing, D., 2002. Reconstructing the spatio-temporal traffic dynamics from stationary detector data. Cooperative Transportation Dyamics 1 (3), 3–1.

Treiber, M., Hennecke, A., Helbing, D., 2000. Congested traffic states in empirical observations and microscopic simulations. Physical Review E 62 (2), 1805.

Treiber, M., Kesting, A., 2012. Validation of traffic flow models with respect to the spatiotemporal evolution of congested traffic patterns. Transportation Research Part C: Emerging Technologies 21 (1), 31–41.

Yeniay, O., 2005. Penalty function methods for constrained optimization with genetic algorithms. Mathematical and Computational Applications 10 (1), 45–56.

Zhao, T., Nie, Y. M., Zhang, Y., 2014. Extended spectral envelope method for detecting and analyzing traffic oscillations. Transportation Research Part B: Methodological 61, 1–16.

Zheng, Z., Ahn, S., Chen, D., Laval, J., 2011. Applications of wavelet transform for analysis of freeway traffic: Bottlenecks, transient traffic, and traffic oscillations. Transportation Research Part B: Methodological 45 (2), 372–384.

Zheng, Z., Ahn, S., Monsere, C., 2010. Impact of traffic oscillations on freeway crash occurrences. Accident Analysis and Prevention 42, 626-636.

Zielke, B. A., Bertini, R. L., Treiber, M., 2008. Empirical measurement of freeway oscillation characteristics: an international comparison. Transportation Research Record: Journal of the Transportation Research Board 2088 (1), 57–67.